Comparing thermoluminescence data on lanthanides in 36 compounds with predictions from vacuum referred binding energy diagrams

Dorenbos, Pieter

DOI
10.1016/j.omx.2024.100316

Publication date
2024

Document Version
Final published version

Published in
Optical Materials: X

Optical Materials: X 22 (2024) 100316

Contents lists available at ScienceDirect

Optical Materials: X

journal homepage: www.elsevier.com/locate/omx

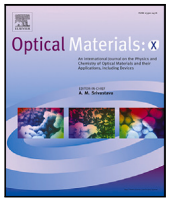

Invited article

Comparing thermoluminescence data on lanthanides in 36 compounds with predictions from vacuum referred binding energy diagrams

Pieter Dorenbos

Delft University of Technology, Faculty of Applied Sciences, Department of Radiation Science and Technology, Mekelweg 15, 2629 JB Delft, Netherlands

ARTICLE INFO

Keywords:
Luminescence
Phosphors
Scintillators
Quantum dots
Nanomaterials
OLED
Glasses
Electroluminesce

ABSTRACT

Thermoluminescence (TL) often involves the liberation of a charge carrier (an electron or a hole) from a charge carrier trapping centre into the conduction band (CB) or the valence band (VB) with subsequent recombination with a counter charge carrier at a luminescence centre. TL glow peak analysis can provide the energy ΔE_t needed to liberate such charge carrier which then defines the location of the charge transition levels (CTL) of the carrier trapping centres below the CB-bottom or above the VB-top. The temperature at the maximum of the TL glow peak changes 3–4 K per 0.01 eV change in ΔE_t thus providing an extremely sensitive probe of energy changes in CTLs. This work collects and reviews data on glow peaks due to electron or hole release from lanthanide dopants in 36 different inorganic compounds. To compare results from different literature sources, data were always re-analysed using the same method that is solely based on the temperature at the maximum of the glow peak. The changes in ΔE_t along the lanthanides series provides insight at the sub 0.1 eV level on the changes in CTL energies. We will use a compound-dependent parameter to account for the nephelauxetic effect and a compound dependent parameter to account for lattice relaxation around the lanthanide. Together with information from lanthanide luminescence spectroscopy, the vacuum referred binding energy (VRBE) diagram will be constructed for each compound. The lanthanide electron or hole trap depth read from the VRBE scheme will be compared with that derived from the TL glow peak. Surprisingly good agreement will be demonstrated.

1. Introduction

The functioning of optical and electronic materials is usually connected to how electrons are transferred between electronic states of the material. This is evident for luminescence phosphors where electrons undergo optical transitions between quantum states of the luminescent species as illustrated for Tb^{3+} with arrows (a) and (b) in Fig. 1. Electron transitions from the valence band (VB) to the conduction band (CB), arrow (1), defines the window of transparency and the bandgap of insulating materials. In solid state batteries, the flow of electrons in the external circuit, the flow of ions through the electrolyte, and attainable battery voltage is intimately connected with the energy involved in reduction and oxidation of the electron storing species [1]. The efficiency of photocatalytic splitting of water into oxygen and hydrogen depends on the location of the VB and CB of the photo-anode with respect to the redox potentials of water [2]. One needs to know the binding energy of a charge carrier during each stage to understand the functioning of the material.

In this work we will limit the discussion to the lanthanide-activated inorganic family of compounds. These are materials that are widely used for application such as luminescent phosphor in lighting systems, as laser crystals, scintillation crystals for the detection of ionizing radiation, charge carrier storage phosphors utilized either as afterglow phosphors, dosimetry phosphors for radiation monitoring, or X-ray storage phosphors in, for example, dental imaging [3,4]. Thermal quenching of luminescence is often controlled by the location of the emitting state with respect to the CB-bottom or the VB-top of the host compound [5]. The charge carrier (an electron or a hole) trapping depth is given by the location of the ground state of the trapping centre with respect to the CB or VB and can be determined with thermoluminescence (TL) techniques [6–8]. In order to understand and to utilize luminescence and carrier trapping phenomena we then need to know the binding energy of an electron in the relevant states with respect to that in the host bands. A most unique property of the lanthanides is that with the filling of the 4f-orbital with at most 14 electrons, the binding energies in the 4f ground states always follow a similar zigzag shape pattern. This is illustrated in Fig. 1.

Vacuum referred binding energy (VRBE) diagrams with the divalent and trivalent lanthanide level energies have gained popularity in the past decade because of their high predictive and explanatory potential. The VRBEs in the lanthanide ground state levels are equivalent to the

E-mail address: p.dorenbos@tudelft.nl.

https://doi.org/10.1016/j.omx.2024.100316
Received 17 January 2024; Received in revised form 6 March 2024; Accepted 4 April 2024
Available online 6 April 2024

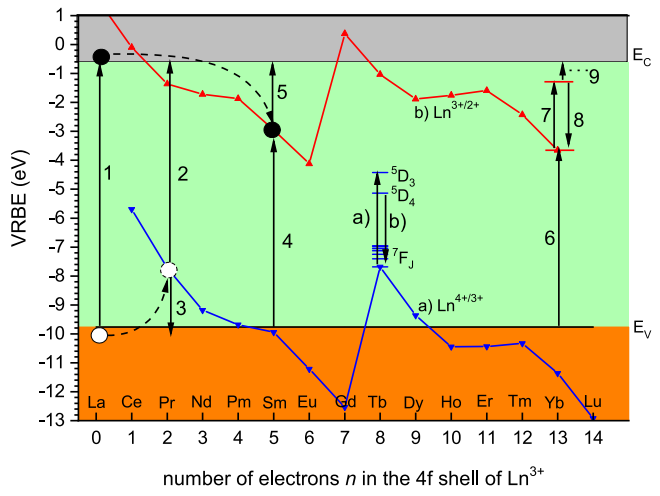

Fig. 1. Vacuum referred binding energy diagram with the location of curve (a) the $Ln^{4+/3+}$ and curve (b) the $Ln^{3+/2+}$ charge transition levels connected with characteristic zigzag solid curves. The arrows indicate various charge carrier transitions that can be experimentally observed.

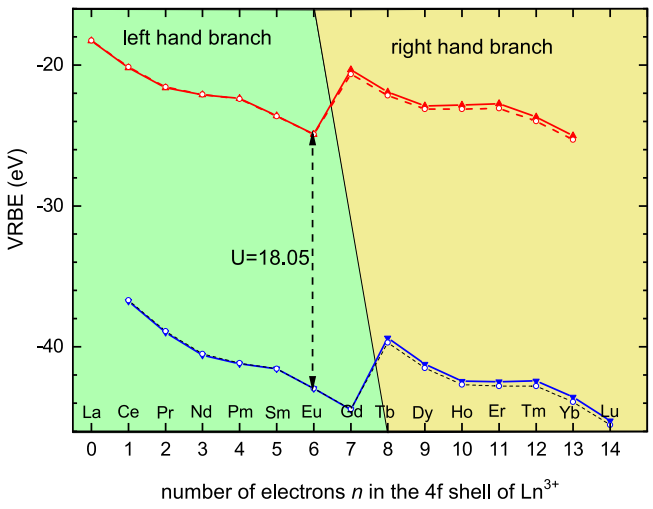

Fig. 2. Free lanthanide CTL-curves as function of the number of electrons in the 4f-orbital. The dashed curve is obtained when inter-electron repulsion is reduced by 6%, i.e., when $\beta = 0.94$. The curves with reduced repulsion are normalized such that for Eu the CTLs coincide with the free ion Eu CTLs. Changes on the left-hand branch are marginal but the right-hand branch is lowered by ≈0.3 eV.

$Ln^{3+/2+}$ and $Ln^{4+/3+}$ charge transition levels (CTL), and they vary in a systematic and thus predictable fashion. At the start of the development of host referred binding energy (HRBE) diagrams [9] and later the VRBE-diagrams [10] various pieces of information on electronic transitions involving lanthanides were combined. Arrows (4) and (6) in Fig. 1 indicate electron transitions from the VB-top to Sm^{3+} and Yb^{3+} thus defining the $Sm^{3+/2+}$ and $Yb^{3+/2+}$ CTLs above the VB-top. Likewise arrow (2) indicating direct excitation of an electron from Pr^{3+} to the CB, defines the $Pr^{4+/3+}$ CTL below the CB-bottom. Arrow (9) indicates the energy barrier for thermal quenching of Yb^{2+} 5d-4f emission due to thermal ionization of the excited state 5d-electron to the CB. Arrow (3) indicates the energy needed to liberate a hole from Pr^{4+} to the VB, and arrow (5) to liberate an electron from Sm^{2+} to the CB as can be obtained from TL studies. Combining such information enables the unravelling of the systematics behind lanthanide CTLs. Now that the method of VRBE-diagram construction is well established, such diagrams can by exploited to predict properties like the energy of charge transfer (CT) bands, the thermal quenching of lanthanide emission, the preferred valence state of a lanthanide, the depth of the electron trap or the hole trap provided by a lanthanide. VRBE-diagrams also provide insight in the VRBE at the conduction band bottom and valence band top and how those change between compounds. This is nowadays frequently utilized in bandgap engineering of phosphor properties, see e.g. [11–13].

It is quite remarkable that with few experimentally determined values, one may already construct a VRBE diagram having all the lanthanide CTLs. The method of VRBE-construction is based on various assumptions, but it is however not yet well established whether those assumptions hold for all type of compounds (halides, oxides, sulphide etc.) alike. Ideally, the energies involved in transitions 3 and 2, 4 and 5, and 6, 7 and 9 in Fig. 1 should all add up to that of transition (1). To spot shortcomings in VRBE-diagram construction, the energy barrier ΔE_q of thermal quenching of lanthanide luminescence was compared with predictions from a VRBE diagram in [5]. In this work we augment that study with the charge carrier trapping depths ΔE_t obtained from TL. Fig. 1 shows that many of the trivalent lanthanides may trap an electron and TL can then probe the energy needed to liberate such electron into the conduction band as illustrated for Sm^{2+} with transition (5). The trivalent lanthanides Ce^{3+}, Pr^{3+} and Tb^{3+} are often able to trap a hole and then TL can probe the location of the $Ln^{4+/3+}$ CTL above the VB. Suppose we excite optically an electron from the VB-top to a Ln^{3+}, one then obtains the location of the $Ln^{3+/2+}$ CTL above the VB-top. One might also first charge the phosphor by trapping an electron from the CB in that same Ln^{3+} to obtain the location of that same $Ln^{3+/2+}$ CTL below the CB-bottom. Ideally, knowing the band gap of the compound both CTLs should coincide. However, one may think of many reasons why it will not be ideal. Do we really optically excite from the VB-top or are there also transitions from somewhere deeper in the VB? With TL we start from a trapped electron state at Ln^{2+} with a fully relaxed lattice around it whereas after CT we end in an unrelaxed state at Ln^{2+}. How will lattice relaxation affect the CTL? Is it really needed that the charge carrier during TL-readout transports via the CB or VB or is some lower energy route possible? By collecting and analysing TL data involving electron and/or hole release from lanthanides we aim to confirm the VRBE schemes or otherwise spot systematic errors.

2. Theory and experimental methods

In this section, first the theory and main idea behind the Chemical Shift model to construct VRBE diagrams will be reviewed. The equations, parameters, and experimental input parameters needed for VRBE construction will be presented. Next the Arrhenius equation describing thermal quenching of luminescence and the Randall-Wilkins equation describing a TL glow peak are treated.

2.1. The chemical shift model and lanthanide charge transition levels

To understand charge transition level energies of the lanthanides in compounds one first needs to treat them as free ions in vacuum. By definition the energies of the free ion $Ln^{3+/2+}$ CTLs are the same as minus the 3rd ionization potentials of the lanthanides. Likewise the free ion $Ln^{4+/3+}$ CTLs are minus the 4th ionization potentials. As illustrated in Fig. 2 the free ion CTLs follow a characteristic double seated zigzag curve with the number of electrons in the 4f-orbital. The shape arises from the Coulomb repulsion between the 4f-electrons when the lanthanides are in their $^{2s+1}L_J$ ground states. The repulsion energies can be obtained from the radial part of the 4f-orbital functions using the refined spin pairing theory of Jørgensen [14,15] together with the experimental Slater–Condon parameters [16,17]. Fig. 2 illustrates what happens with the free ion CTL shapes when the 4f-4f inter electron repulsion is reduced by 6%. For $n < 8$, i.e., the left-hand branch of the CTL curve, change in CTL is insignificant. However, for $n > 7$ defining the right-hand branch, the entire branch is lowered by ≈0.3 eV.

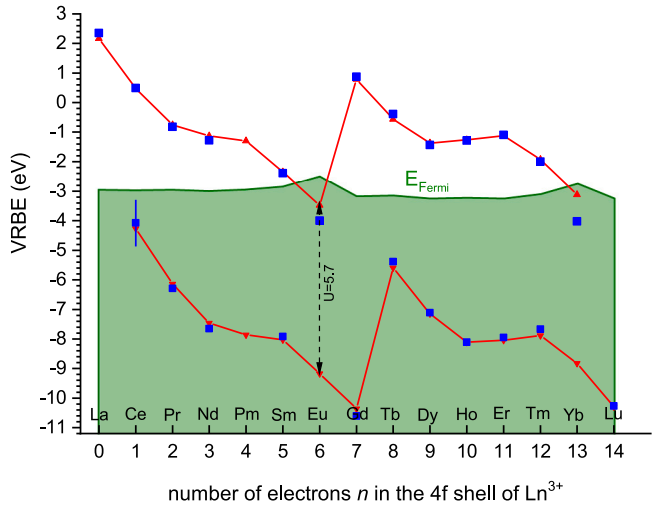

Fig. 3. The $Ln^{3+/2+}$ and $Ln^{4+/3+}$ CTLs in the pure lanthanide metals as derived from photoelectron spectroscopy when CTLs are below the Fermi level, and inverse photoelectron spectroscopy when they are above. The Fermi energy E_F is obtained from reported values for the work function. See [10] for further details. The solid curves connect the CTLs obtained with the RCS-model using $U = 5.7$ eV, $\beta(2+) = \beta(3+) = 0.91$, $f(2+) = f(3+) = 0.68$ corresponding with $\alpha(2+) = 0.11$ eV/pm and $\alpha(3+) = 0.18$ eV/pm.

Let us now place the lanthanides in a compound. The positively charged lanthanides will then be surrounded by negative charge which adds a Coulomb repulsion to the 4f-electrons. As a result, the entire CTL curve is moved upwards with an amount known as the chemical shift. The Chemical Shift model states that a divalent lanthanide is effectively surrounded (screened) by 2- electronic charge at average screening distance close to the lanthanide ionic radius, and a trivalent lanthanide likewise by 3- electronic charge [10]. The chemical shift for trivalent lanthanides is then roughly 3/2 larger than for divalent ones. This implies that the energy difference between the two CTL curves will decrease when in compounds. The absolute size of the chemical shift depends on how close the surrounding screening charge can approach the lanthanide, i.e., the screening distance. Screening is most perfect, and approach is most close in the pure lanthanide metals where the di- or trivalent lanthanide cation is surrounded by 2 or 3 free conduction band electrons in each unit cell of the metal. Chemical shift will then be maximum with minimum energy separation between the two CTL curves.

Fig. 3 shows the CTLs of the lanthanides in the pure lanthanide metals. Data points below the Fermi level were derived from photoelectron spectroscopy and above from inverse photoelectron spectroscopy. Data were reviewed and analysed in [10]. The two solid zigzag curves connecting the CTLs are obtained with the Refined Chemical Shift (RSC) model [16,17]. We will express the separation between the two CTL curves with the U-value for Eu, defined as the energy difference between the CTL of $Eu^{3+/2+}$ and $Eu^{4+/3+}$. It is 18.05 eV in vacuum as in Fig. 2 and has reduced to (5.7 ± 0.1) eV for Eu-metal in Fig. 3.

In inorganic compounds, the surrounding electrons are bonded in the anions and the anions are bonded in the crystalline lattice. This bonding will resist the free movement of surrounding screening charge and the chemical shift will be smaller and the U-value larger than for metals. The U-value for a compound can be derived when sufficient spectroscopic data is available for several different lanthanides in the same compound. It appears largest (7.6–7.4 eV) for fluoride compounds where electrons are strongly bonded in the highly electronegative fluorine [18,19]. It decreases progressively with weaker bonding of the electrons and anions until the limiting case of 5.7 eV for the lanthanide metals is reached. Although U can be determined experimentally, it has proved very difficult to establish the chemical shift and therewith the energies of the CTLs with respect to the vacuum level.

Matters changed with the development of the Chemical Shift model published in 2012 [10,20]. The model not only explains the origin of chemical shift and how it depends on compound properties but also proposes the following relation between the $U(A)$-value for compound A and the size of the chemical shift,

$$CTL(Eu^{3+/2+}, A) = -24.92 + \frac{18.05 - U(A)}{0.777 - 0.0353U(A)} \quad (1)$$

and

$$CTL(Eu^{4+/3+}, A) = CTL(Eu^{3+/2+}, A) - U(A) \quad (2)$$

where the last term in Eq. (1) is the chemical shift $E_{cs}(Eu, 2+, A)$ of the $Eu^{3+/2+}$ CTL in compound A, and 24.92 eV is the third ionization potential of Eu. In [16,17] everything was put together in one equation to represent all $Ln^{4+/3+}$ and $Ln^{3+/2+}$ CTL energies

$$\begin{aligned} CTL(Ln^{Q+1/Q}, A) =& C(q, Q) + \beta(Q, A)S(q, Q) + (1 - \beta(Q, A)S(Eu, Q)) \\ &+ E_{cs}(Eu, Q, A) \\ &+ \alpha(Q, A)(R(Eu, Q) - R(q, Q)) \end{aligned} \quad (3)$$

where q the number of electrons in the 4f-orbital. $S(q, Q)$ is a function that accounts for the main features in the CTL curves of the free lanthanides and that has been calculated by combining Jørgensen spin pairing theory with experimentally derived Slater–Condon F^k parameters [16]. $C(q, Q)$ appears a smoothly decreasing function with increasing q and obtained by subtracting $S(q, Q)$ from the ionization potentials, see Fig. SI-1 and Fig. SI-2. $R(q, Q)$ are the ionic radii of the lanthanides. $R(Eu, Q)$ represents the ionic radius $R(6, 3+)$ in case of Eu^{3+} or $R(7, 2+)$ in case of Eu^{2+}. $C(q, Q,)$, $S(q, Q)$, $R(q, Q)$ are constants that were tabulated in [16,17] and reproduced in Table 1. In the case Ln=Eu, Eq. (3) becomes identical to Eq. (1) for $Q = 2+$ and Eq. (2) for $Q = 3+$. The parameter $\beta(Q, A)$ accounts for the nephelauxetic effect. $\beta = 1$ for the free lanthanides, 0.94 for the example in Fig. 2, and 0.91 for the lanthanide metals in Fig. 3. In this work we will frequently use as first estimate for $\beta(2+)$ and $\beta(3+)$

$$\beta(2+, A) = \beta(3+, A) = 0.656 + 0.04 \times U(A) \quad (4)$$

$\alpha(Q, A)$ are the contraction tilt parameters in eV/pm. The function $C(q, Q)$ might change slightly with chemical environment although it is expected to remain a smoothly decreasing function with q. Unfortunately, this cannot be tested experimentally. We will therefore use the $C(q, Q)$ values in Table 1 for all environments and a slight dependence with A is then absorbed in the value for $\alpha(Q, A)$ and chemical shift. Note that the term $(1-\beta(Q, A)S(Eu, Q))$ in Eq. (3) was absent in the equations presented in [16,17]. That omission was a mistake, but fortunately in all VRBE diagrams presented after introduction of the RCS-model the correct Eq. (3) was used.

Fig. 4 shows the CTLs of the lanthanides when $U = 7.09$ eV which applies for YPO_4. The chemical shift for Eu^{2+} amounts 20.8 eV and for Eu^{3+} it is 31.8 eV. Their ratio of 1.53 is close to 3/2. To arrive at the CTLs for the other lanthanides, we need to account for the lanthanide contraction. In going from La to Lu, the ionic radius decreases by about 12% [21] as can be seen in Table 1. When the lanthanide is placed on a site in a compound, the surrounding screening charge can approach the smaller lanthanide more closely than the larger one. The chemical shift will then increase with smaller size of the lanthanide. Assuming that the effect is linear with the ionic radius, the entire CTL-curve will be tilted counter clockwise as illustrated in Fig. 4. This tilting is expressed with the contraction tilt parameters $\alpha(Q, A)$ in the last term of Eq. (3). In [10], the contraction tilt in eV/pm and the Eu chemical shift $E_{cs}(Eu, Q, A)$ were related as

$$\alpha(Q, A) \approx \frac{f(Q, A)}{1440Q}(E_{cs}(Eu, Q, A))^2 = \frac{f(Q, A)}{1440Q}\left(\frac{18.05 - U(A)}{0.777 - 0.0353U(A)}\right)^2 \quad (5)$$

The relaxation fractions $f(Q, A) < 1$ were introduced because in lanthanide doped inorganic compounds, lattice relaxation does not

Table 1
The energies C and S, and the lanthanide ionic radii R needed to compute the $Ln^{4+/3+}$ and $Ln^{3+/2+}$ charge transition level energies with the Refined Chemical Shift model. q is the number of electrons in the 4f-orbital of the divalent lanthanides and n in the trivalent ones. Energies are in eV and radii in pm.

q	n	Ln	$R(q,2+)$	$R(n,3+)$	$C(q,2+)$	$S(q,2+)$	$C(n,3+)$	$S(n,3+)$
1	0	La	148.7	–	−18.170	−0.116	–	–
2	1	Ce	147.0	128.26	−19.723	−0.475	−36.591	−0.167
3	2	Pr	145.3	126.58	−21.087	−0.537	−38.370	−0.610
4	3	Nd	143.7	124.97	−22.325	0.223	−39.895	−0.705
5	4	Pm	142.2	123.42	−23.331	0.962	−41.387	0.187
6	5	Sm	140.7	121.94	−24.390	0.789	−42.627	1.072
7	6	Eu	139.3	120.53	−25.249	0.329	−43.870	0.900
8	7	Gd	137.9	119.19	−25.901	5.566	−44.852	0.402
9	8	Tb	136.6	117.91	−26.535	4.625	−45.792	6.422
10	9	Dy	135.4	116.7	−27.084	4.194	−46.712	5.487
11	10	Ho	134.3	115.55	−27.809	4.969	−47.524	5.089
12	11	Er	133.2	114.47	−28.569	5.829	−48.478	5.998
13	12	Tm	132.2	113.46	−29.243	5.563	−49.375	6.955
14	13	Yb	131.3	112.52	−29.913	4.883	−50.191	6.631
–	14	Lu	–	111.7	–	–	−51.066	5.816

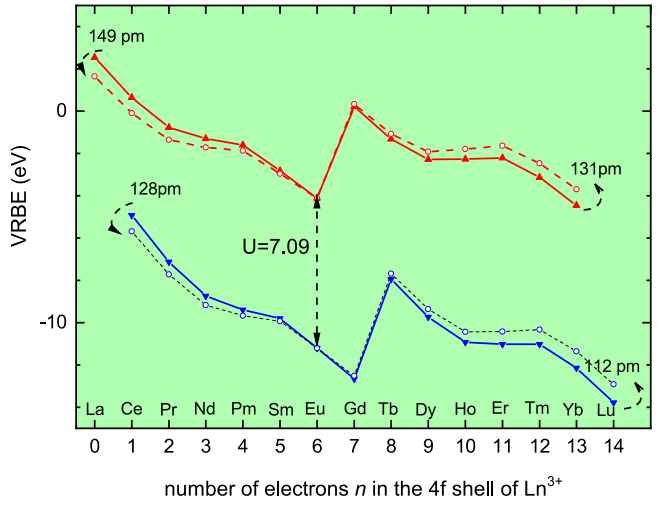

Fig. 4. CTL curves for U = 7.09 eV and $\beta(3+)$ = 0.94 and $\beta(2+)$ = 0.95. The solid curves are without tilt correction or $\alpha(2+) = \alpha(3+) = 0$. The dashed curves are with $\alpha(2+)$ = 0.095 eV/pm and $\alpha(3+)$ = 0.098 eV/pm causing a slight counter clockwise rotation due to the lanthanide contraction. The ionic radius of the lanthanides at the start and end of the CTL curves are provided.

fully compensate for the ionic radius difference between the lanthanide and the cation it has substituted for. For the pure lanthanide metals in Fig. 3, we used $f(2+,\text{metal}) = f(3+,\text{metal}) = 0.68$ yielding $\alpha(2+,\text{metal}) = 0.11$ eV/pm and $\alpha(3+,\text{metal}) = 0.18$ eV/pm where the ratio of 1.64 is slightly larger than 3/2. For the compounds of this work we will find that with $f(2+,A)$ in the range 0.58–0.72 and $f(3+,A)$ in the range 0.42–0.45 good agreement with available experimental data from TL studies is obtained.

With Eq. (5), Eq. (1), Eq. (2), and Eq. (4), we arrive at a situation that we need only the $U(A)$ value and the two $f(Q,A)$ values for our compound to establish all $Ln^{3+/2+}$ and $Ln^{4+/3+}$ CTL energies in that compound. Next task is to find the VRBE at the VB-top and the CB-bottom. There are many techniques to establish those energies with respect to the lanthanide CTL. Most important method is to use the so-called charge transfer (CT) band energy $E^{CT}(Eu^{3+},A)$ that appears in the excitation spectra of Eu^{3+} emission. Here an electron is transferred from the top of the VB to Eu^{3+} that is then converted into Eu^{2+}. The VRBE E_V at the VB-top is then given by

$$E_V(A) = CTL(Eu^{3+/2+},A) - E^{CT}(Eu^{3+},A). \quad (6)$$

Information on Eu^{3+} is most abundant but one may equally well use the CT-band energy to another trivalent lanthanide like indicated by arrows (4) and (6) in Fig. 1, and use the CTL for that lanthanide instead. However, in presenting the parameters used in VRBE construction we will always specify the value for the VB→Eu^{3+} CT either measured for Eu^{3+} or derived from the CT energy to another Ln^{3+} by using the shape of the CTL curve as given by Eq. (3). To arrive at the VRBE at the CB-bottom we must add the mobility band gap energy to E_V

$$E_C(A) = E_V(A) + E^{ex}(A) + 0.008(E^{ex}(A))^2 \quad (7)$$

where $E^{ex}(A)$ is the energy of exciton creation and $0.008(E^{ex})^2$ an empirical estimate for the electron–hole binding energy in the exciton as was proposed in [22].

The effect of temperature on CTL energies has been disregarded in the past. However, the glow peak temperature in TL recordings may cover a temperature range of 100 to 1000 K and the same applies to the thermal quenching temperature of lanthanide luminescence. Then in order to use derived trapping depths and quenching energy barriers to verify VRBE schemes one may not disregard temperature anymore. Due to lattice expansion and electron phonon interaction, the CTL energies of the lanthanides and that of E_V and E_C depend on temperature. This aspect was studied in Ref. [23] where it was found that cation CTLs move down and anion CTLs move up by several 0.1 eV when temperature increases from 10 K to RT. The transitions labelled (1), (3), (4), and (6) in Fig. 1 all concern charge carrier transfer between an anion and a cation. Those energies decrease slightly when temperature increases. This was demonstrated by comparing experimental data on E^{ex} and on $E^{CT}(Eu^{3+})$ at 10 K and RT. The temperature dependence of E^{CT} can roughly be represented by

$$E^{CT}(T) = E^{CT}(293K) - 6\times10^{-4}(T-293). \quad (8)$$

Although there appears quite some compound-to-compound variation in that dependence, we will use this equation to correct values to the RT situation.

The transitions labelled (2), (5), (9) concern electron transfer between a lanthanide cation and the cation derived states at the CB-bottom. The energies of those states shift in the same direction when temperature changes. Although they shift not necessarily in the same pace, we will assume that the transition energies are independent on temperature and there is no need for correcting to the RT situation.

In using the parameter E^{CT} employed for VRBE construction there was never attention for the temperature. Usually, an average value from data reported in literature was taken that may be at RT or at lower temperature. For E^{ex} usually the value pertaining around 10 K was used. With such method errors of the order of few 0.1 eV are introduced in the VRBE scheme which was thought acceptable considering other errors in VRBE construction. Anyway, all VRBE schemes of this work will be based on the E^{ex} and E^{CT} values that pertain to RT. Whenever experimental data were measured at another temperature, they were corrected to the RT values using the findings in [23].

Finally we have arrived at the three main parameters $U(A)$, $E^{CT}(Eu^{3+},A)$, and $E^{ex}(A)$ pertaining to 293 K that provide all necessary information to construct the room temperature VRBE scheme for compound A with E_V, E_C, and the $Eu^{3+/2+}$ and $Eu^{4+/3+}$ CTLs. The values for $\beta(Q,A)$ and $f(Q,A)$ are then needed together with Eqs. (3) and (5) to obtain the CTLs for all other lanthanides than Eu.

2.2. The Arrhenius and Randall-Wilkins equation

In [5], the quenching of lanthanide $4f^n$-$4f^n$ emission due to thermally activated electron transfer from the Pr^{3+} $^3P_0$ level and the Tb^{3+} $^5D_4$ level to the conduction band, and due to thermally activated hole transfer from the Eu^{3+} $^5D_0$ level to the valence band was studied. In addition the quenching of $4f^{n-1}5d$-$4f^n$ emission of Eu^{2+} and Ce^{3+} which often (if not always) proceeds by electron transfer to the conduction band was studied. In all five cases the quenching involves a charge carrier transfer from an excited state to E_V or E_C, and then the energy difference between the lanthanide CTLs and E_V or E_C is crucial. The

Table 2
The dependence of T_{50} on the activation energy ΔE_q in K/eV calculated for $\Gamma_0 = 2\times 10^{13}$ Hz and using the typical value for τ_v in column 4. The bottom row relates to lanthanide TL glow peaks in YPO_4 where $T_m/\Delta E_t = 314$ K/eV when the heating rate $\beta = 0.1$ K/s. Column six compiles the energy offset values in eV.

A	Transition	$\lambda(nm)$	τ_v	$T_{50}/\Delta E_q$	ΔE_{offset}
Ce^{3+}	$5d \rightarrow 4f[^2F_{5/2,7/2}]$	300–550	40 ns	850	0.0 ± 0.2
Eu^{2+}	$5d \rightarrow 4f[^8S_{7/2}]$	380–600	1000 ns	690	−0.15 ± 0.15
Pr^{3+}	$^3P_0 \rightarrow {}^3H_{4,5,6}$	490, 550, 620	50 μs	560	0.3 ± 0.15
Tb^{3+}	$^5D_4 \rightarrow {}^7F_5$	≈545	2 ms	475	0.5 ± 0.15
Eu^{3+}	$^5D_0 \rightarrow {}^7F_{1,2}$	≈610	2 ms	475	0.45 ± 0.12
TL	YPO_4	$G = 14.6$	$\beta = 0.1$	314	–

aim of [5] was twofold; (i) to derive the quenching energy barrier ΔE_q from published luminescence data by using the Arrhenius equation, (ii) to explore if and how it agrees with prediction from constructed VRBE schemes employing the RCS-model. In this work we will employ published TL data with similar aims; (i) to derive the charge carrier trapping depths ΔE_t by using the Randall-Wilkins equation describing a TL glow peak, and (ii) to explore if or how it agrees with prediction from constructed VRBE schemes employing the RCS-model. The combined studies give a strong experimental support for the method of VRBE construction but also reveals the limitations of the method.

The thermal quenching of luminescence intensity $I(T)$ is traditionally expressed with the single energy barrier Arrhenius equation

$$I(T) = \frac{I(0)}{1 + \frac{\Gamma_0}{\Gamma_v} exp(\frac{-\Delta E_q}{kT})} \quad (9)$$

where Γ_v is the radiative decay rate, Γ_0 is the attempt rate for thermal quenching which is assumed to have similar magnitude as the maximum phonon frequency in compounds, k is the Boltzmann constant. However, in the case when there is not a single energy barrier ΔE_q but instead a barrier height distribution, Eq. (9) will provide wrong results. In the presence of a symmetrical distribution, the quenching curve shape will become less steep but the temperature T_{50} where luminescence intensity has dropped by 50% remains practically the same. Rather than fitting quenching curves with Eq. (9) it is then better to choose a reasonable value for Γ_0 based on the composition of the compound, and then derive ΔE_q from the temperature T_{50}. For that, equation

$$T_{50} = \frac{11600}{\ln(\tau_v \Gamma_0)} \Delta E_q \quad (10)$$

applies where $\tau_v = 1/\Gamma_v$. Now we should interpret ΔE_q as the average energy of the distribution.

Table 2 shows the studied transitions of the five lanthanides in [5] with the typical decay times. With longer decay time Eq. (10) predicts the rate of change of T_{50} with ΔE_q to decrease. For the fast decay 5d-4f emission of Ce^{3+} it is as large as 850 K/eV and for the slow decay of the 4f-4f emission in Tb^{3+} and Eu^{3+} it reduces to 475 K/eV. In [5] data on T_{50} was gathered from the archival literature covering more than 170 different compounds. For each compound, the quenching energy barrier ΔE_q was determined from a constructed vacuum referred binding energy diagram (VRBE). Data were reanalyzed for Eu^{3+} in [23]. For Eu^{3+}, Pr^{3+}, and Tb^{3+}, the data follow the predicted rate of change reasonably well. For Eu^{2+} and Ce^{3+} correlation was less evident because of strong scatter of data points.

When T_{50} approaches 0 K, one expects the quenching energy barrier ΔE_{VRBE} as read from the VRBE diagram to approach zero too. However, experimentally an offset energy ΔE_{offset} is observed and

$$\Delta E_{VRBE} = \Delta E_{offset} + \frac{T_{50} \ln(\tau_v \Gamma_0)}{11600}. \quad (11)$$

Those offset energies are compiled in column 6 of Table 2. For example, in the case of Tb^{3+} the quenching energy barrier added to the $^5D_4$ level location in the band gap leads on average to an energy of about $\Delta E_{offset} = (0.5 \pm 0.15)$ eV below E_C. These values will be used in the discussion section to assess the accuracy and systematic errors in VRBE diagrams.

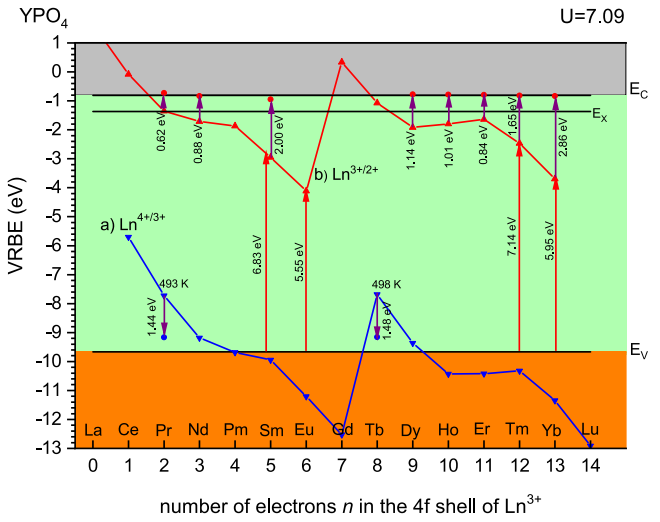

Fig. 5. The room temperature vacuum referred binding energy scheme for the trivalent and divalent $4f^n$ lanthanide ground state levels in YPO_4. (a) Connects the VRBE in the Ln^{3+} $4f^n$ ground state levels and can also be denoted as the $Ln^{4+/3+}$ charge transition levels, (b) connects the same for divalent lanthanides. E_V, E_X, E_C are the VRBE at the valence band top, in the host exciton state, and at the conduction band bottom, respectively. Observed energies for VB→Ln^{3+} CT, electron trap depths, and hole trap depths are written along the drawn arrows. The endpoints are indicated by solid bullet data symbols near E_C and E_V.

When thermal quenching of lanthanide luminescence involves the thermally excited electron or hole transfer from an excited lanthanide state to a host band, the physical processes are similar as with thermoluminescence when an electron or hole is thermally excited from the lanthanide ground state to the host band. Fig. 5 shows the room temperature VRBE diagram for the lanthanides in YPO_4 as constructed with the RCS-model [10,16,17]. It shows that the ground states of the divalent lanthanides Pr^{2+} until Yb^{2+} are 0.5 to 3.0 eV below the CB-bottom which means that the corresponding trivalent lanthanides form 0.5 to 3.0 eV deep electron traps. Similarly, the ground state of Ce^{3+}, Pr^{3+}, and Tb^{3+} are several eV above the VB-top and they from stable traps for holes generated in the VB. One may then combine a deep hole trap like Ce^{3+} with a shallower electron trap like Pr^{3+} until Yb^{3+} to systematically study electron release from Ln^{2+} with TL techniques. First studies were performed in 2008 by Bos et al. [24], and several studies on this system followed [25–27]. Fig. 6 shows the sequence of TL glow curves for YPO_4:Ce^{3+};Ln^{3+} from data in [26]. First the phosphor was charged by β-irradiation creating holes in the VB that are trapped to form Ce^{4+} and creating electrons in the CB that are trapped to form divalent lanthanides. Next the phosphor is heated linearly with time at a rate of $\beta = 0.1$ K/s. The TL intensity $I(T)$ from Ce^{3+} 5d-4f emission shows typical glow curves with initially an exponential rise, followed by the maximum at temperature T_m and then dropping rapidly towards zero. One may also replace Ce^{3+} for another hole trap like Pr^{3+} or Tb^{3+} to obtain the same sequence of glow peaks but then with recombination luminescence from Pr^{3+} or Tb^{3+} [26,27].

Solving the rate equations describing the thermally activated release of a charge carrier from a trap of depth ΔE_t when a sample is heated at a linear rate of β K/s one obtains, assuming first order recombination kinetics, the Randall-Wilkins equation for the TL intensity $I(T)$ as function of temperature [6–8],

$$I(T) = n_0 \frac{s}{\beta} \exp(-\frac{\Delta E_t}{kT}) \exp[-\frac{s}{\beta} \int_{T_0}^{T} \exp(-\frac{\Delta E_t}{kT'}) dT'] \quad (12)$$

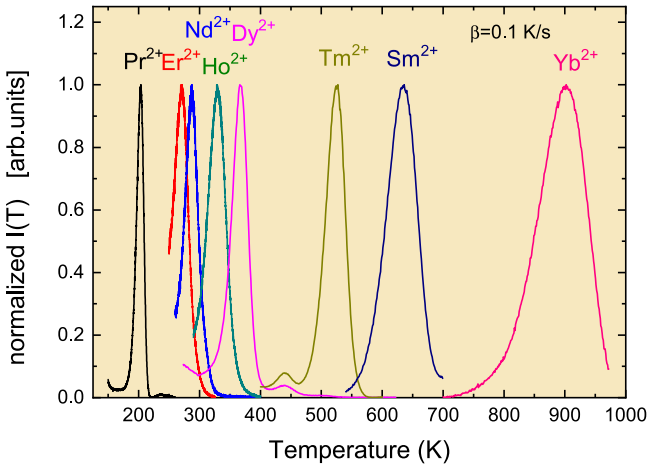

Fig. 6. The TL glow curves for YPO_4:Ce^{3+};Ln^{3+} phosphors at heating rate β = 0.1 K/s as measured in [26].

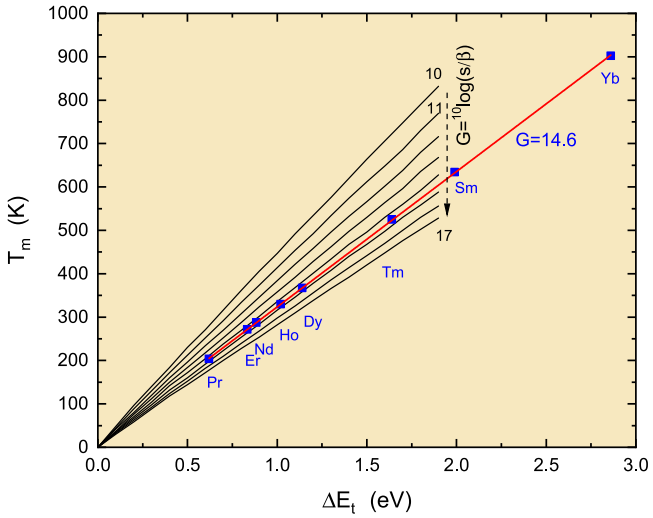

Fig. 7. The temperature T_m as function of ΔE_t derived from the Randall-Wilkins equation for values $G = ^{10}\log(s/\beta)$ ranging 10, 11, 12, .. to 17. The data symbols refer to results from TL-glow peaks of YPO_4:Ce^{3+};Ln^{3+} for G = 14.6.

where n_0 the number of traps that were filled during the preceding charging phase, s is the same as Γ_0 that appears in the Arrhenius equation Eq. (9), and k the Boltzmann constant. The first exponential describes the exponential rise of the glow peak, and the second exponential the rapid drop towards zero. From Eq. (12) one may derive a relation for the temperature T_m at the maximum of the glow peak

$$\frac{\beta \Delta E_t}{kT_m^2} = s\exp(-\frac{\Delta E_t}{kT_m}) \quad (13)$$

with the materials parameter s and ΔE_t.

Using simple models, s can be related to the maximum phonon frequency ν_0, a transition probability κ to the delocalized state, and a term that contains the entropy change ΔS upon delocalizing the charge carrier [8],

$$s = \nu_0 \kappa \exp(\frac{-\Delta S}{k}). \quad (14)$$

Problem is that we do not know how to evaluate κ and ΔS. Besides, we do not know to what extend Eq. (14) really applies and alternative theories are still being developed [28]. In this work we will simply assume that $s = \nu_0$ which depending on the compound ranges from 4×10^{12} Hz to 4×10^{13} Hz [29]. Note that the precise value for s is not essential since a factor of 100 difference only results in a 0.05 eV different trap depth evaluated with Eq. (13).

Fig. 7 shows how T_m changes with ΔE_t for various values of $G \equiv ^{10}\log(s/\beta)$ where β in TL recordings falls usually between 0.05 K/s and 5 K/s. Almost perfect proportional relations emerge with proportionality constants from 300 K/eV to 400 K/eV. The data points in Fig. 7 are from the results of YPO_4:Ce^{3+};Ln^{3+} in Fig. 6. Assuming $s = 4 \times 10^{13}$ Hz or G = 14.6 when β = 0.1 K/s, the ΔE_t were derived from the T_m values using Eq. (13). A linear fit through the data provides a slope of 314 K/eV with an intercept at 11.4 K for ΔE_t = 0. The intercept demonstrates that for very small ΔE_t, T_m is not strictly proportional to ΔE_t anymore. The 314 K/eV result for YPO_4 is also listed in the last row of Table 2 to demonstrate similarity with thermal quenching. The value of 314 K/eV would also have been obtained in the case of luminescence quenching when $\tau_v \approx$ = 550 s. Translated to a TL-recording this is the typical time needed to record a TL-glow of about 55 K width at a heating rate of 0.1 K/s.

The problem with using Eq. (12) is that in practice the trap depth ΔE_t will not be single valued but there will be a trap depth distribution around an average, just like with the Arrhenius equation to describe thermal quenching of luminescence. Examples can be found in [30–33]. Likewise, there is not much point in fitting a TL-glow peak with the idealized first order RW-equation. One may exploit methods and techniques like the initial rise method, peak cleaning techniques and variable heating rate plot to extract information from TL [8,24]. In this work we will follow a more practical route. In the presence of a distribution of ΔE_t or other then first order recombination kinetics, the shape of the TL-glow will broaden. Fortunately, Eq. (13) appears to hold also quite well when ΔE_t is interpreted as the average trap depth [34]. Because T_m varies proportionally with ΔE_t and the TL-glow peak is apart from the exponential rise reasonably symmetric, the temperature T_m does not change dramatically in the presence of a distribution. The glow peak will just broaden. Again this is quite similar as with the T_{50} value from the thermal quenching curve of luminescence. Given the heating rate β together with a reasonable estimate for s, one may then directly obtain ΔE_t from the observed value of T_m. This is the method that will be followed throughout this work.

The ΔE_t derived from the observed T_m in Fig. 6 should correlate with the energy difference between the CB-bottom of YPO_4 and the $Ln^{3+/2+}$ CTL. The obtained e-trap depths are shown in Fig. 5 with the vertical arrows starting at the $Ln^{3+/2+}$ CTL. Apart from Sm^{2+} they all end within 0.1 eV from the CB-bottom at E_C = −0.81 eV. Note that the T_m values range from 200 K to 900 K, and over such 700 K temperature range the VRBE energy at the CB-bottom and of the $Ln^{3+/2+}$ CTL will change. This aspect was further treated in [23] where it was concluded that the CB-bottom and the $Ln^{3+/2+}$ CTL shift in the same direction when temperature changes thus not affecting the e-trap depth too much. This is now reconfirmed with the results in Fig. 5. In the Results section below, we will collect TL-data from the archival literature to derive the electron and hole trapping depths of lanthanides. For each compound the room temperature VRBE diagram will be constructed, and the experimental trapping depths will be compared with what the VRBE scheme predicts. The aim is to prove, on the one hand, the consistency between experiment and prediction and, on the other hand, to unveil systematic errors or shortcomings in VRBE diagram construction.

3. Results

A general problem with TL-curves is how to assign an observed TL-glow peak to a specific electron releasing or hole releasing defect. There are always trapping centres in a compound of which the nature and the location of their CTLs are not known beforehand. Even in the case of intentionally doped materials often the location of the CTLs of the dopants are not known. How then to decide which glow peak belongs to

Table 3
The parameters used for room temperature VRBE diagram construction where compounds are arranged in sequence of decreasing U-value together with the obtained E_V and E_C values. All energies are in eV. The errors in U, $E^{CT}(Eu^{3+})$, and E^{ex} are estimated typically ±0.1 eV.

A	U	E^{CT}	E_V	E^{ex}	E_C	$\beta(2+)$	$\beta(3+)$	$f(2+)$	$f(3+)$
free Ln	18.05		–		–	1.000	1.000	0.000	0.000
$NaLaF_4$	7.51	7.72	−12.05	10.28	−0.92	0.956	0.956	0.582	0.425
$LaPO_4$	7.18	4.84	−9.00	7.95	−0.54	0.943	0.943	0.582	0.425
$NaYP_2O_7$	7.18	5.46	−9.62	7.82	−1.31	0.943	0.943	0.582	0.425
$GdPO_4$	7.13	5.15	−9.28	8.00	−0.77	0.941	0.941	0.582	0.425
YPO_4	7.09	5.55	−9.66	8.30	−0.81	0.950	0.940	0.630	0.425
$LuPO_4$	7.08	5.65	−9.76	8.55	−0.62	0.939	0.939	0.617	0.425
$Sr_2MgSi_2O_7$	7.03	4.56	−8.64	7.20	−1.03	0.937	0.937	0.582	0.425
$MgGeO_3$	7.00	4.75	−8.82	5.93	−2.61	0.950	0.936	0.651	0.425
$LiLuGeO_4$	6.95	5.21	−9.25	6.25	−2.69	0.934	0.934	0.582	0.425
$NaLuGeO_4$	6.95	5.35	−9.39	6.33	−2.74	0.934	0.934	0.582	0.425
$NaYGeO_4$	6.94	5.33	−9.37	6.23	−2.83	0.934	0.934	0.582	0.425
$Ca_2MgSi_2O_7$	6.91	4.56	−8.58	7.00	−1.19	0.950	0.934	0.617	0.425
$LiScGeO_4$	6.90	5.56	−9.58	6.40	−2.85	0.932	0.932	0.582	0.425
$LiLuSiO_4$	6.90	5.37	−9.39	7.30	−1.66	0.940	0.932	0.651	0.425
$Gd_3Ga_5O_{12}$	6.90	5.02	−9.04	5.70	−3.08	0.932	0.932	0.582	0.425
$LiYSiO_4$	6.89	5.32	−9.33	7.40	−1.49	0.950	0.932	0.685	0.425
$Ca_3Si_2O_7$	6.88	5.10	−9.11	6.78	−1.96	0.940	0.931	0.617	0.425
$Gd_3AlGa_4O_{12}$	6.88	5.00	−9.01	5.97	−2.75	0.931	0.931	0.617	0.425
$Gd_3Al_2Ga_3O_{12}$	6.86	5.20	−9.20	6.08	−2.82	0.930	0.930	0.617	0.425
$Lu_3Al_2Ga_3O_{12}$	6.85	5.40	−9.39	6.50	−2.56	0.940	0.930	0.617	0.425
$Gd_3Sc_2Ga_3O_{12}$	6.84	4.77	−8.76	6.00	−2.47	0.930	0.930	0.617	0.425
$Y_3Al_2Ga_3O_{12}$	6.80	5.19	−9.16	6.33	−2.51	0.940	0.928	0.617	0.425
$Y_3Al_5O_{12}$	6.77	5.45	−9.40	6.85	−2.18	0.940	0.927	0.616	0.425
$LaAlO_3$	6.76	3.90	−7.85	5.95	−1.62	0.926	0.926	0.582	0.425
$GdAlO_3$	6.75	4.75	−8.69	7.30	−0.97	0.930	0.926	0.685	0.425
Sr_3SiO_5	6.74	3.76	−7.70	6.15	−1.25	0.940	0.926	0.651	0.425
$SrSi_2O_2N_2$	6.70	3.38	−7.30	6.20	−0.79	0.924	0.924	0.685	0.425
$LiTaO_3$	6.70	4.57	−8.49	5.44	−2.81	0.922	0.922	0.617	0.425
MgO	6.60	5.27	−9.14	7.54	−1.15	0.920	0.920	0.582	0.425
$YSiO_2N$	6.60	3.80	−7.67	5.90	−1.49	0.924	0.924	0.617	0.425
$SrSi_2AlO_2N_3$	6.60	2.85	−6.72	5.44	−1.05	0.925	0.920	0.685	0.425
Lu_2O_2S	6.40	3.72	−7.50	4.63	−2.70	0.912	0.912	0.582	0.425
Y_2O_2S	6.37	3.76	−7.53	4.68	−2.67	0.911	0.911	0.582	0.445
Gd_2O_2S	6.35	3.72	−7.48	4.68	−2.62	0.910	0.910	0.582	0.445
$Ca_2Si_5N_8$	6.35	2.98	−6.74	5.05	−1.48	0.930	0.930	0.719	0.445
La_2O_2S	6.30	3.64	−7.37	4.61	−2.59	0.908	0.915	0.582	0.445
Ln-metal	5.70		–		–	0.910	0.910	0.680	0.680

a lanthanide and which to a defect, and whether it is from hole release or from electron release? Since the invent of HRBE and VRBE schemes involving the lanthanides, we have a means to establish the location of the lanthanide CTLs. However, accuracy is limited to several 0.1 eV and knowing that the T_m of glow peaks may shift by 30–40 K/0.1 eV, this still makes assignment of TL-glow peaks to specific lanthanide trapping centres not trivial. Matters became manageable when combining TL studies on various combinations of lanthanides with HRBE and VRBE schemes as in Fig. 5. We learned from such schemes that the $Ce^{4+/3+}$ CTL in wide bandgap compounds is always several eV above the VB-top making Ce^{4+} a stable hole trap. When combining Ce^{3+} with a Ln^{3+} as in Fig. 6 one observes with TL studies Ce^{3+} emission which implies that the Ln^{3+} acted as an electron trap and the glow is from e-release with recombination at Ce^{4+}. One may also combine the hole trap Pr^{3+} with the deeper electron trap of Eu^{3+}. In such case with TL studies the hole is released from Pr^{4+} to recombine with Eu^{2+} resulting in Eu^{3+} emission. Thus by studying different combinations of lanthanides in the same compound one may eventually evidence that an observed glow peak is from e-release or h-release and assign it to a specific lanthanide dopant.

Since the work on YPO_4, many other compounds with lanthanides were studied by TL. These data have been collected and re-analysed to derive the trapping energies. In total information from 36 different lanthanide doped compounds were found. For each compound information on the energies E^{ex} and $E^{CT}(Ln^{3+})$ was gathered from published spectroscopic data. In each case the values that apply at room temperature were used. In cases that only information at e.g. 10 K was available, a correction to RT was made using the methods in [23] and Eq. (8) for $E^{CT}(T)$. For the exciton binding energy, the last term of Eq. (7) was used. The U-value was obtained with the methods outlined in [35]. When the centroid shift of the Ce^{3+} 4f-5d transitions is known, as for YPO_4, the U-value was derived from that centroid shift and will be denoted as U_c. In cases when the compound contains only one type of anion, the estimator tool based on the average cation electronegativity χ_{av} of the compound in [35] was used. Such U-value will be denoted as U_X. For the compounds with two types of anions the method of a weighted average of single anion compounds was followed [35] and denoted as U_w. All parameters used for constructing the VRBE diagrams are compiled in Table 3 along with the energies E_V and E_C obtained with Eqs. (6) and (7).

The VRBE diagram for each compound in the same style as the one for YPO_4 in Fig. 5 can be found in Fig. SI-3 until Fig. SI-14. Fig. 8 shows a stacked VRBE diagram of the 36 compounds in Table 3 together

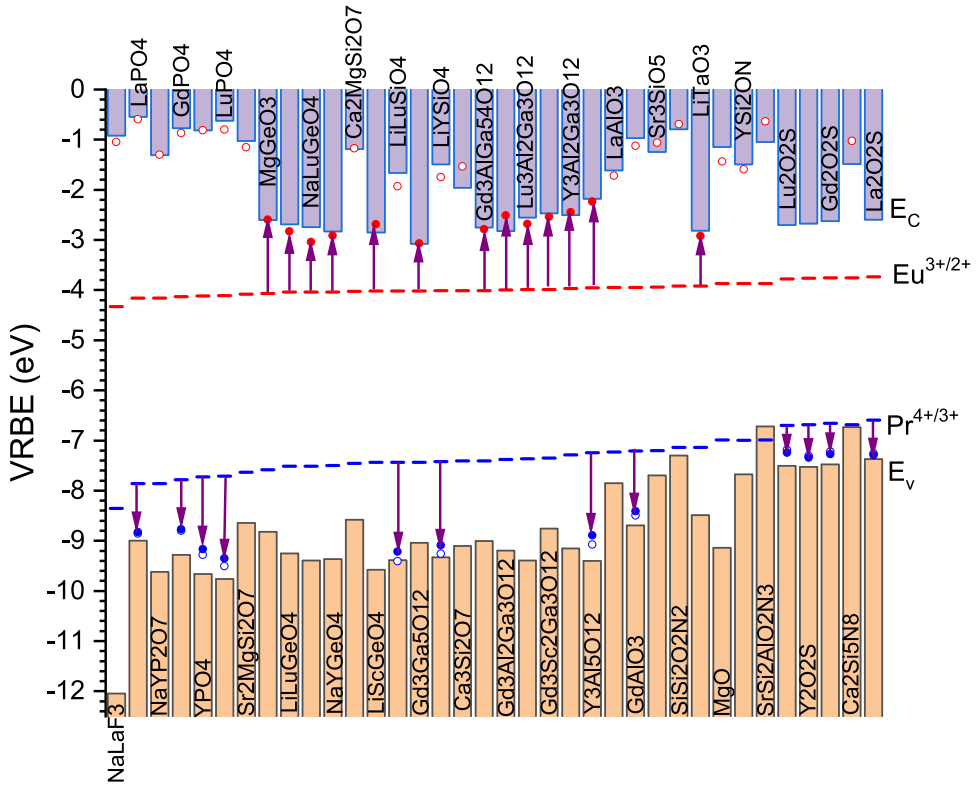

Fig. 8. Stacked VRBE diagram with the $Eu^{3+/2+}$ and $Pr^{4+/3+}$ CTLs of the 36 compounds of this study. Upward pointing arrows starting at the $Eu^{3+/2+}$ CTLs have length equal to the Eu^{2+} e-trap depths. The solid bullet data points are the endpoint energies. The open bullet data points near E_C mark the average endpoint energies derived from e-trap depths from divalent lanthanides other than Eu^{2+}. Downward pointing arrows starting at the $Pr^{4+/3+}$ CTLs have length equal to the Pr^{4+} h-trap depths at temperature T_m. The solid bullet data points are the endpoint energies. The open bullet data points near E_V are the endpoint energies when a correction to RT is made.

with the CTLs of $Pr^{4+/3+}$ and $Eu^{3+/2+}$. Compounds are arranged in sequence of decreasing U-value and therefore increasing chemical shift and increasing energy of the CTLs.

3.1. Lanthanide electron trapping depths

Table 4 compiles the compounds and references where TL-curves with glow peaks due to release of an electron from a divalent lanthanide was reported. The temperatures T_m at the maxima of the observed glow peak together with the used TL heating rate β and the used hole trapping and recombination centre can be found in Table SI-I. Using Eq. (13), the e-trap depth ΔE_t^e was derived from T_m, β and the value for s. The obtained values for ΔE_t^e together with the used s are compiled in Table 4. Here, one should regard ΔE_t^e as a measure for the average value of an unknown trap depth distribution.

Depending on the location of the $Ln^{3+/2+}$ CTL curve with respect to the energy E_C at the CB-bottom different trivalent lanthanides may act as an electron trap. For the compound YPO_4 we have information on the e-trap depths of 8 different lanthanides. The glow peaks were shown in Fig. 6 and the e-trap depth values in Table 4 were used in Fig. 7. Fig. 5 shows that the CTLs for $La^{3+/2+}$, $Ce^{3+/2+}$ and $Gd^{3+/2+}$ are inside the CB and those lanthanides are not able to trap an electron in the 4f-orbital. Here we have to note that the ground state electron configuration for these divalent lanthanides will be $4f^n5d$ and not $4f^{n+1}$, and the genuine CTLs will be at lower energy. The $Eu^{3+/2+}$ CTL is very deep below the CB-bottom and a TL-glow peak from the Eu^{2+} e-trap would be located well above 1000 K and beyond the range of TL-readers. Eu^{2+} e-trap depths are only available on compounds, with a low lying CB-bottom. The stacked diagram of Fig. 8 shows that in seven garnet compounds, five germanate compounds, and in $LiTaO_3$, the CB-bottom is in the range −2.2 eV to −3.2 eV. Those are the compounds in Table 4 where glow peaks have been attributed to the Eu^{2+} and Yb^{2+} e-traps. The VRBE diagrams of those compounds in Fig. SI-3 until Fig. SI-14 show that the $Ln^{3+/2+}$ CTLs of all other lanthanide are well inside the CB and electron trapping is not possible. For $SrSi_2O_2N_2$ two sets of e-trap values are listed in Table 4 for the lanthanides Dy, Ho, and Er. For each lanthanide, the TL-curve shows a strong glow peak accompanied by a weak satellite glow peak at higher temperature [58], see also Table SI-I. Apparently, there are two sites for the lanthanides with differing e-trap depths. The ones responsible for the satellite glow peaks have 0.14 eV deeper e-traps. In Fig. SI-11c, we suggest that the two sites differ in the $Ln^{3+/2+}$ CTL energies. Similar applies for $Ca_3Si_2O_7$ where Ueda et al. [49] observe double e-release glow peaks for Sm^{2+} and Tm^{2+}. Table 4 and Fig. SI-8b show that they differ about 0.23 eV in energy. One may interpret this as site dependent $Ln^{3+/2+}$ CTL energies. However, it is also possible that a fraction of the e-trap defects is close neighbour to the h-trap defects. Coulomb attraction between trapped electron and trapped hole combined with local lattice distortions may facilitate the TL-recombination leading to lower e-trap depths.

3.2. Lanthanide hole trapping depths

The VRBE scheme for the wide bandgap compound YPO_4 in Fig. 5 shows that only Ce^{3+}, Pr^{3+}, and Tb^{3+} are deep hole trapping centres and this applies for most oxide based compounds. A TL glow peak has never been assigned to hole release from Ce^{4+} in an oxide compound. The trap is just too deep to generate a glow peak below say 1000 K. Only hole release from Pr^{4+} and Tb^{4+} has been reported. The used heating rates β and observed glow peak maxima T_m together with the used electron trapping and recombination centre can be found in Table SI-II. Table 5 compiles the h-trap depths of Pr^{4+} and Tb^{4+} derived from T_m using the value for β and the listed frequency factors s.

For the oxide compounds in Table 5, the h-trap depths ΔE_t^h for Pr^{4+} and Tb^{4+} appear in the range 0.6 to 1.8 eV. In the four oxysulfide

Table 4
The depth ΔE_t^e of the electron trap in eV on a divalent lanthanide in compounds as derived from the temperature T_m at the maximum of the glow peak. The used frequency factor s is in units of 10^{13} Hz.

A	s	Pr^{2+}	Nd^{2+}	Sm^{2+}	Eu^{2+}	Dy^{2+}	Ho^{2+}	Er^{2+}	Tm^{2+}	Yb^{2+}	Ref.
$NaLaF_4$	1.5			2					1.77		[36]
$LaPO_4$	4		1.21	2.31		1.49	1.32	1.18	1.92		[37]
$NaYP_2O_7$	4			1.75		0.65	0.47				[38]
$GdPO_4$	4						1.02				[37]
YPO_4	4	0.62	0.88	2		1.14	1.01	0.84	1.65	2.86	[26]
$LuPO_4$	4			2.07		1.18	1.03	1	1.71		[39]
$Sr_2MgSi_2O_7$	2.5								1.4		[40]
$MgGeO_3$	2.5				1.47					0.95	[41]
$LiLuGeO_4$	2.5				1.21						[42]
$NaLuGeO_4$	2.5				1						[43,44]
$NaYGeO_4$	2.5				1.12						[43]
$Ca_2MgSi_2O_7$	2.5			1.73					1.16		[45]
$LiScGeO_4$	2.5				1.33						[42]
$LiLuSiO_4$	2.5			1					0.4		[46]
$Gd_3Ga_5O_{12}$	1.5				0.95						[47,48]
$LiYSiO_4$	2.5			1.15					0.52		[46]
$Ca_3Si_2O_7$(stronger)	2.85			1.12					0.62		[49]
$Ca_3Si_2O_7$(weaker)	2.85			1.37					0.83		[49]
$Gd_3AlGa_4O_{12}$	1.5				1.22						[47]
$Gd_3Al_2Ga_3O_{12}$	1.5				1.49						[47]
$Lu_3Al_2Ga_3O_{12}$	1.5				1.31					0.99	[50]
$Gd_3Sc_2Ga_3O_{12}$	1.5				1.45					≈0.99	[51]
$Y_3Al_2Ga_3O_{12}$	1.5				1.52					1.04	[52,53]
$Y_3Al_5O_{12}$	1.7				1.72					1.31	[54]
$LaAlO_3$	1.7			1.03					0.79		[55]
$GdAlO_3$	1.7		0.45			0.69	0.54	0.4	1.17		[56]
Sr_3SiO_5	2.5			1.83					1.15		[57]
$SrSi_2O_2N_2$(stronger)	2.5					1.13	0.99	0.85			[58]
$SrSi_2O_2N_2$(weaker)	2.5					1.27	1.12	0.99			[58]
$LiTaO_3$	2.5				1						[59]
MgO	1.5			1.23					0.93	2.03	[60,61]
$YSiO_2N$	1.5			1.15					≈0.84		[33]
$SrSi_2AlO_2N_3$	2.5		1.02			1.06	0.9	0.75	>1.71		[62]
$Ca_2Si_5N_8$	2.5		0.45			0.52			1.03		[63,64]

Table 5
The depth ΔE_t^h of the hole trap in eV on Pr^{4+} and on Tb^{+} in compounds as derived from the temperature T_m at the maximum of the glow peak. The used frequency factor s is in units of 10^{13} Hz.

A	s	Pr^{4+}	Tb^{4+}	Ref.
$LaPO_4$	4	0.97	1.01	[37,65]
$LaPO_4$	4	0.6	0.69	[37,65]
$GdPO_4$	4	0.99	0.99	[65]
$GdPO_4$	4	0.76	0.81	[65]
YPO_4	4	1.44	1.48	[26,37]
$LuPO_4$	4	1.64	1.68	[37]
$LiLuSiO_4$	2.5	1.78	1.79	[46]
$LiYSiO_4$	2.5	1.65	1.68	[46]
$Y_3Al_5O_{12}$	1.7	1.65	1.61	[54,66]
$GdAlO_3$	1.7	1.22	1.18	[56]
Lu_2O_2S	1.4	0.55	0.46	[67]
Y_2O_2S	1.3	0.66	0.6	[67]
Gd_2O_2S	1.3	0.62	0.56	[67]
La_2O_2S	1.1	0.7	0.68	[67]

compounds the trap depth is shallow and around 0.6 eV. This is due to the presence of the sulphide anion leading to a high VRBE at the VB-top as can be seen in the stacked diagram of Fig. 8. In the case of $LaPO_4$ and $GdPO_4$, two sets of hole trap depths are listed in Table 5. $LaPO_4$:Pr^{3+};Eu^{3+} and $LaPO_4$:Tb^{3+};Eu^{3+} were studied by Lyu and Dorenbos [37] and the TL-curves are reproduced in Fig. 9. Here Eu^{3+} acts as the deep electron trap and Pr^{3+} and Tb^{3+} as the less deep hole traps. During TL-readout, the hole is released from Pr^{4+} or Tb^{4+} to recombine at Eu^{2+} generating Eu^{3+} emission. The glow peaks IIIa and IIIb were attributed to hole release from Tb^{4+} and Pr^{4+} and glow peaks IIa and IIb to hole release from unknown defects. In this work we also assign peaks IIa and IIb to hole release from Pr^{4+} and Tb^{4+} but at sites providing about 0.33 eV deeper h-traps than those responsible for glow peaks IIIa and IIIb. Similar situation exists for $GdPO_4$, and the two sets of hole trap depths, differing about 0.2 eV, are listed in Table 5.

4. Discussion

The results on e-trap depths and h-trap depths in Table 4 and 5 will be used three-fold. (1) We will analyse the relative variation in trap depth in going through the lanthanide series. That variation follows the shape of the zigzag lanthanide CTL-curves of Eq. (3). Because TL is a highly sensitive technique we will use the compiled data to critically analyse that shape and compound to compound variations therein. This analysis will provide information on the relaxation fractions $f(Q,A)$ of relevance for the tilt parameters $\alpha(Q,A)$ and will provide information on the nephelauxetic parameters $\beta(Q,A)$. (2) The trap depth expresses the location of the CTL with respect to the VB or CB of the host compound. We will focus on the e-trap depth of Eu^{2+} as representative for the $Ln^{3+/2+}$ CTL-curve, and on the h-trap depth of

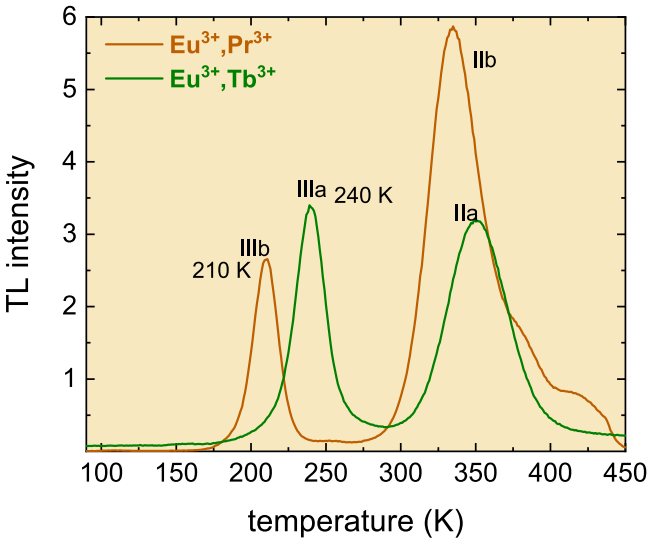

Fig. 9. The TL glow curves for $LaPO_4$:Pr^{3+};Eu^{3+} and $LaPO_4$:Tb^{3+};Eu^{3+} monitoring Eu^{3+} emission at a heating rate β = 1 K/s as measured in [37].

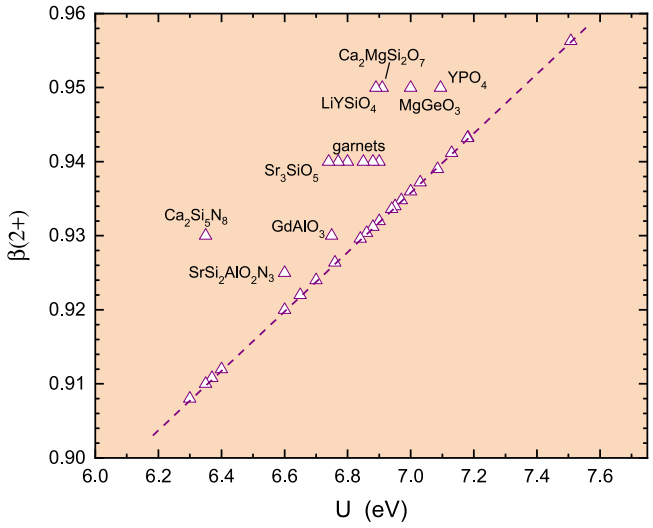

Fig. 10. Values for $\beta(2+)$ used to construct the VRBE schemes.

Pr^{4+} as representative for the $Ln^{4+/3+}$ CTL-curve. Ideally the e-trap depth added to the $Eu^{3+/2+}$ CTL should coincide with the CB-bottom and similarly the h-trap depth subtracted from the $Pr^{4+/3+}$ CTL should coincide with the VB-top. This analysis will provide insight in the consistency between the parameters U, E^{ex}, and E^{CT} with observed trapping depths. (3) With TL-studies, the thermally excited release of charge carriers from the lanthanide ground states are probed. With studies on thermal quenching of lanthanide emission, the thermally excited release of charge carriers from excited states are probed. Both should be consistent with each other and with the VRBE diagram.

4.1. The shape of the $Ln^{3+/2+}$ and $Ln^{4+/3+}$ CTL-curves

In the RCS-model, the shape of the lanthanide CTL curves is given by Eq. (3). It is foremost based on the free lanthanide ion CTL curves as shown in Fig. 2. These curves are being tilted when in compounds as shown in Fig. 4. The relaxation fractions $f(Q,A)$ provide the tilt parameters $\alpha(Q,A)$ in Eq. (5) which is then used in Eq. (3). In addition we have the nephelauxetic parameters $\beta(Q,A)$ which causes a lowering of the right hand branch with several 0.1 eV as demonstrated in Fig. 2. By definition $\beta = 1$ for the free lanthanides and it may reduce to values around 0.91 for highly covalent compounds like the selenides. As first approximation Eq. (4) will be used to estimate β. Next, one may change the values slightly to attain best agreement between the $Ln^{Q+1/Q}$ CTL shapes and the observed trap depths. For the relaxation fractions, we start as first approximation with $f(2+) = 0.63$ and $f(3+) = 0.425$. Again values can be slightly modified to attain best agreement between the $Ln^{Q+1/Q}$ CTL shapes and the observed trap depths. The chosen set of values for each compound can be found in Table 3.

YPO_4 is the compound with most information on e-trap depths for different lanthanides. Only then it is feasible to deduce a unique set of $\beta(2+)$ and $f(2+)$ values. However, in most cases we know e-trap depths of only one or two lanthanides, and then it becomes difficult or impossible to find a unique combination. We then tend to choose values close to the starting values. Fig. 10 shows the chosen values for $\beta(2+)$ in Table 3 where the dashed line is given by Eq. (4). Often the values for $\beta(3+)$ were chosen equal to that for $\beta(2+)$.

There are 5 compounds in Table 4 where we can compare the e-trap depth of Dy^{2+} from the right hand branch of the CTL curve with that of Nd^{2+} from the left hand branch. With decrease of U-value, $\beta(2+)$ tends to decrease and the right hand branch will lower with respect to the left hand branch. This predicts that the Dy^{2+} to Nd^{2+} trap depth difference should increase. However, the opposite appears to be the case. It is 0.28 eV, 0.26 eV, 0.24 eV, 0.04 eV, and 0.07 eV for $LaPO_4$, YPO_4, $GdAlO_3$, $SrSi_2AlO_2N_3$, and $Ca_2Si_5N_8$. With decrease of the U-value, the chemical shift increases and with Eq. (5) the tilt parameter $\alpha(2+)$ tends to increase, and that will have an opposite effect on the Dy^{2+} to Nd^{2+} trap depth difference. It seems then that, the parameter $\alpha(2+)$ is more important for the energy differences than the parameters β.

TL data on hole release from Pr^{4+} from the left hand branch and Tb^{4+} from the right hand branch in 8 different compounds were already presented and analysed in [17]. Table 5 reproduces the same 8 compounds plus in addition recent data on the RE_2O_2S (RE = La, Gd, Y, Lu) from [67]. A trend is observed with decrease of U-value in the h-trap depth differences between Pr^{4+} and Tb^{4+}. Tb^{4+} appears a 0.04–0.09 eV deeper h-trap than Pr^{4+} in $LaPO_4$ but in the RE_2O_2S it is 0.02–0.09 eV more shallow. Apparently when U decreases from 7.2 to 6.3 eV, the $Tb^{4+/3+}$ CTL moves down by ≈ 0.15 eV with respect to that of $Pr^{4+/3+}$. Values for $\beta(3+)$ and $f(3+)$ listed for the compounds in Table 5 were chosen such that the h-trap depth difference between Pr^{4+} and Tb^{4+} agrees within 0.02 eV with experiment. Apart from La_2O_2S, we used Eq. (4) to choose $\beta(3+)$. $f(3+)$ was kept at 0.425 as much as possible. Only for three oxysulphides we needed to choose a somewhat larger value of 0.445.

The observation that the f and β values remain always fairly close to the starting estimated values implies that generally the trap depths closely follow the CTL shapes from the RCS-model. However, we also have to conclude that they still may deviate 0.1–0.2 eV. A likely reason is uncertainty in the value for $f(Q,A)$ that determines the tilt factor $\alpha(Q,A)$ in Eq. (5). The amount of lattice relaxation around a lanthanide dopant on a site in a compound is usually not known and can/will differ from compound to compound. Furthermore, introducing $f(Q,A)$ was under the assumption that each bondlength from a lanthanide to its neighbouring anion changes with the same fraction (breathing mode type of relaxation), and also that those fractions are the same for each lanthanide. Both are not necessarily true. It is well possible that one coordinating anion relaxes much more than others. It all depends on crystal structure and bonding. One may even imagine that $f(Q,A)$ for the larger lanthanides at the beginning of the lanthanide series has different value than at the end of the series. Such dependence would distort the CTL curves beyond what can be accounted for with Eq. (3). It will be clear that we are then hitting the limits of our VRBE construction methods. In addition, we have seen for $Ca_3Si_2O_7$ and $SrSi_2O_2N_2$ the presence of two different sites with different e-trap depths and similar for $LaPO_4$ and $GdPO_4$ with different h-trap depths.

In each VRBE diagram of Fig. SI-3 until Fig. SI-14 and also for YPO_4 in Fig. 5, the e-trap depth added to the $Ln^{3+/2+}$ CTL energy is indicated by a data symbol. We will call that the endpoint energy. The same is done for the h-trap depths subtracted from the $Ln^{4+/3+}$ CTLs. Ideally the endpoint energies for different lanthanides in the same compound should have the same energy. For YPO_4 in Fig. 5 this is very nicely confirmed but also for most of the other compounds in Fig. SI-3 until Fig. SI-14. This all confirms that the TL trap depths follow very nicely the shape of the $Ln^{Q+1,Q}$ CTL curves. Some endpoint energies may deviate as for Sm^{2+} in $NaYP_2O_7$ (see Fig. SI-3c) and Sr_3SiO_5 (see Fig. SI-11b), Tm^{2+} in $LiLuSiO_4$ (see Fig. SI-7b) and $LiYSiO_4$ (see Fig.SI-8a), and Yb^{2+} in $Gd_3Sc_2Ga_3O_{12}$ (see Fig. SI-9c). Deviations are then 0.1–0.4 eV large, but for all other cases the endpoint energies are all within 0.1 eV from each other. We regard this as a confirmation and as evidence that Eq. (3) from the RCS-model provides a correct description of the $Ln^{Q+1/Q}$ CTL curves. The assumption that the relaxation fractions $f(Q, A)$ for a compound are the same for each lanthanide and for each lanthanide-ligand bond is not necessarily correct. Since we do not have the means to establish those fractions for an individual compound, the assumption leads to an unavoidable error source in CTL energies of the order of several 0.1 eV. This entails then a fundamental contribution to the errors in VRBE diagram construction.

4.2. Comparing TL trap-depth and VRBE trap depth

The shapes of CTL curves together with its limitations and errors are quite well established and validated. Next step is to assess its location with respect to the host bands and the vacuum level. For that, we will use the e-trap depth data for Eu^{2+} and the hole trap depth data for Pr^{3+} both from the left hand branch of the CTL-curves. Ideally,

$$E_V + E^{CT}(Eu^{3+}, RT) + \Delta E_t^e(Eu^{2+}) = E_C \tag{15}$$

and

$$E_V + E^{CT}(Eu^{3+}, RT) - U + (5.50 - 1.51 \times \beta(3+) + 6.05 \times \alpha(3+)) - \Delta E_t^h(Pr^{4+}) = E_V \tag{16}$$

where in the latter equation the term between the braces is the energy difference between the $Eu^{4+/3+}$ and $Pr^{4+/3+}$ CTL energies from Eq. (3).

The lengths of the upward pointing arrows starting at the $Eu^{3+/2+}$ CTL energy in Fig. 8, and also in the corresponding VRBE diagrams in Fig. SI-3 until SI-14, represent the $\Delta E_t^e(Eu^{2+})$ e-trap depths from Table 4. The endpoints of the arrows, indicated by solid bullet data symbols, are the energies on the left hand side of Eq. (15) which should ideally coincide with the CB-bottom. Often, they are surprisingly close to E_C with strongest deviation for $NaLuGeO_4$ (Fig. SI-6a) and $Gd_3Al_2Ga_3O_{12}$ (Fig. SI-9a). The endpoint energies for e-traps other than that of Eu^{3+} can be found in the VRBE diagrams of Fig. SI-3 until Fig. SI-14. The endpoint energies averaged over different lanthanides for each compound are shown as open bullet data symbols in the stacked diagram of Fig. 8. Again, most endpoints are within few tenths of an eV from E_C. Relatively large deviations (up to 0.3–0.4 eV) occur for the compounds $LiLuSiO_4$ (Fig. SI-7b), $LiYSiO_4$ (Fig. SI-8a), $Ca_3Si_2O_7$ (Fig. SI-8b), MgO (Fig. SI-12b), $SrSi_2AlO_2N_3$ (Fig. SI-13a), and $Ca_2Si_5N_8$ (Fig. SI-14b). This may signal errors in the used parameters E^{ex} and E^{CT} for VRBE diagram construction. Particularly, E^{ex} = 6.78 eV for $Ca_3Si_2O_7$ from [49] is ≈0.5 eV lower than usually reported for a pyro-silicate compound. The same compound also showed a quenching energy barrier ΔE_q for Eu^{2+} 5d-4f emission that deviates about 0.5 eV from the VRBE diagram prediction in the study of [5]. An 0.5 eV larger E^{ex} will therefore bring the VRBE diagram consistent with both the observed e-trap depths and quenching energy barrier.

The length of the downward pointing arrows starting at the $Pr^{4+/3+}$ CTL energy in Fig. 8 represent the $\Delta E_t^h(Pr^{4+})$ h-trap depths from Table 5. The endpoints are again indicated by solid bullet data symbols and are equivalent to the energies on the left hand side of Eq. (16). The same can be seen in the VRBE diagrams of Fig. SI-3 until SI-14. Ideally, they should coincide with the valence band top E_V as expressed with Eq. (16). However, apart from La_2O_2S they always end at higher energy. This can be explained partly by the temperature dependence of CTL energies. Eq. (8) expresses that with increase of temperature the CTL energy difference between the VB-top and the $Eu^{3+/2+}$ CTL decreases. Assuming a similar dependence for the energy difference between the VB-top and the $Pr^{4+/3+}$ CTL energy one obtains

$$\Delta E_t^h(Pr, 293K) = \Delta E_t^h(Pr, T_m) + 6 \times 10^{-4}(T_m - 293) \tag{17}$$

The open bullet data symbols near E_V in the stacked diagram of Fig. 8 are the endpoint energies when Eq. (17) is applied. The situation improves somewhat but still the endpoint energies tend to be located significantly above the VB-top. This was noticed earlier and attributed to the phenomenon that a hole state at the VB-top tends to be shared by a few neighbouring anions that relax around the hole thus forming a self-trapped hole centre. The self-trapped hole state may then, depending on type of compound, be located 0.3–0.6 eV above the VB-top. It can migrate through the lattice by a hopping type of motion to eventually recombine with the trapped electron. Other possible explanations are suggested by Eq. (16). Perhaps the U-value is systematically underestimated or the energy of the Eu^{3+} CT-band is systematically overestimated. Although the latter would according to Eq. (15) also affect the endpoint energies of the e-trap.

4.3. Systematic errors and mismatches in VRBE diagrams

Ideally the quenching energy barriers ΔE_q derived from lanthanide luminescence quenching data and the e-trap and h-trap depths ΔE_t derived with TL-recordings should agree with what is read from a VRBE diagram. Column 6 of Table 2 and Eq. (11) shows the offsets or mismatch energies in ΔE_q for the lanthanides studied in [5]. These offsets are used in Fig. 11 to illustrate how the results from quenching data mismatch with predictions from the VRBE schemes. The figure shows a VRBE scheme for a hypothetical compound, and the only relevant information are the averaged mismatch energies. For example the 0.3 eV wide shaded bar around the solid bullet data point for Tb^{3+} at 0.5 eV below E_C indicates that, averaged over compounds, the quenching energy barrier ΔE_q added to the $^5D_4$ level location of Tb^{3+} has an endpoint energy of (0.50 ± 0.15) eV below E_C. Information from Table 2 for quenching data for Ce^{3+}, Pr^{3+}, Eu^{3+} are also shown. Furthermore, we have added in the diagram the results from the hole trap depths of Pr^{4+} and Tb^{4+} that on average have an endpoint energy 0.23 eV and 0.24 eV above E_V, and the e-trap depths of divalent lanthanides that on average are an insignificant amount of 0.02 eV different from E_C.

There are errors in the derived trapping depths from TL-glow peaks due to errors in the used value for s, the value for T_m, and the assumption of a symmetrical distribution in trap depths. A factor of 100 error in s or 20 K error in T_m contributes 0.05 eV error in the derived trap depths. Errors of 0.1 eV are present in the U, E^{ex} and E^{CT} parameters needed for VRBE diagram construction. Considering this, the mismatch energies in Fig. 11 are all quite acceptable. An argument that the U-values are systematically underestimated by a few 0.1 eV will lower the mismatches near the VB-top but those for the electron transitions from Ce^{3+}, Pr^{3+} and Tb^{3+} will also lower further below the CB-bottom. So this argument will not provide better overall agreement. In VRBE diagram construction, the energy at the maximum of the Eu^{3+} CT-band is used to place the $Eu^{3+/2+}$ CTL above E_V. This assumption may also have a systematic error. Perhaps one should take an energy slightly beyond or before the maximum. Such error would raise or lower all mismatch energies in Fig. 11 with the same amount. Again, that will not lead to an overall better agreement. Perhaps the differences are supposed to be so. We already discussed the possibility of hole migration by means of a trapped hole centre to explain the

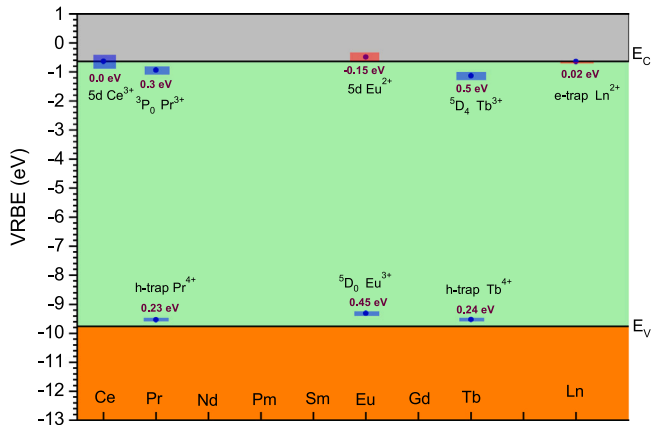

Fig. 11. VRBE scheme of a hypothetical compound. Solid bullet data points mark the average energy differences between energies derived from thermal quenching or TL data and VRBE schemes. The width of the shaded bars indicate error margins. Those near the CB-bottom are obtained from thermal excitation of electrons from Ln^{2+} ground states in TL-recordings or from excited states (5d for Ce^{3+} and Eu^{2+}, $^3P_0$ for Pr^{3+} and $^5D_4$ for Tb^{3+}) in thermal luminescence quenching studies. Those near the VB-top are from thermal excitation of holes from the ground state in the case of Pr^{4+} and Tb^{4+} or from the $^5D_0$ excited state in the case of Eu^{3+}.

on average 0.23 eV mismatch for Pr^{4+}. In the case of quenching or 5d-4f emission for Ce^{3+} and Eu^{2+}, lattice relaxation and Stokes shift contribute to the mismatch energies.

5. Summary and conclusions

This work has collected TL-data on lanthanides in inorganic compounds from the archival literature with the aim to extract information on lanthanide electron or hole trap depths. Since there is always a distribution in trap depths, a method that derives trap depths from the temperature T_m where the glow peaks have maximal intensity was regarded as most appropriate. Information on 36 different compounds were found, and for each compound the room temperature VRBE diagram has been constructed using the RCS-model. The change in electron trap depth with changing type of Ln^{2+} follows the shape of the $Ln^{3+/2+}$ CTL curve usually within 0.1 eV, and this provides further evidence that the variation in CTL energy as obtained with the RCS-model is correct. The electron trap depths added to the Ln^{2+} CTL energy is usually within 0.1 eV from the CB-bottom. In cases where compounds or specific Ln^{2+} show large deviation, there is strong suspicion that there are errors in the construction parameters of the VRBE diagram or that a glow peak has been wrongly assigned to a lanthanide electron trap. The hole trap depth of Pr^{4+} and Tb^{4+} subtracted from the $Pr^{4+/3+}$ and $Tb^{4+/3+}$ CTL energy appears always significantly, i.e. 0.3–0.5 eV, above the VB-top. This is partly attributed to a hole trap depth reduction at the temperature T_m. Self trapped hole centre creation has also been suggested as possible cause.

The results on trap depths ΔE_t from TL data from this work together with data on the energy ΔE_q from thermal quenching of lanthanide luminescence from [5] was compared with the energies as predicted from the VRBE diagrams. There are several error contributions; (1) the parameters E^{ex}, E^{CT}, and U for room temperature VRBE diagram construction may each contain ±0.1 eV error, (2) it is assumed that the relaxation fractions $f(Q, A)$ are the same for each lanthanide and the same for each individual lanthanide-anion bond in the compound. This is not necessarily the case, and it will then distort the lanthanide CTL zigzag curves, (3) lattice relaxation after luminescence excitation and after a valence change of a lanthanide by charge carrier transfer is not accounted for in VRBE diagram construction. (4) An error of 20 K in T_m or a factor of 100 error in the frequency factor s leads to typically 0.05 eV error in the trap depth. This work has shown that the thermal quenching data and charge carrier trapping data are consistent with the predictions from the VRBE schemes. Deviations are of the order of 0.1 to 0.3 eV, and considering the various error contributions one may not expect to have reached better agreement. This means that the method of VRBE diagram construction has been further confirmed with the results of this work.

CRediT authorship contribution statement

Pieter Dorenbos: Writing – review & editing, Writing – original draft, Methodology, Investigation, Formal analysis, Conceptualization.

Declaration of competing interest

The authors declare that they have no known competing financial interests or personal relationships that could have appeared to influence the work reported in this paper.

Data availability

Data will be made available on request.

Appendix A. Supplementary data

Supplementary material related to this article can be found online at https://doi.org/10.1016/j.omx.2024.100316.

References

[1] John B. Goodenough, Youngsik Kim, Chem. Mater. 22 (2010) 587.
[2] Michael G. Walter, Emily L. Warren, James R. McKone, Shannon W. Boettcher, Qixi Mi, Elizabeth A. Santori, Nathan S. Lewis, Chem. Rev. 110 (2010) 6446.
[3] A.J.J. Bos, Nucl. Instr. Meth. B 184 (2001) 3.
[4] K. van den Eeckhout, P.F. Smet, D. Poelman, Materials 3 (2010) 2536.
[5] P. Dorenbos, J. Mater. Chem. C 11 (2023) 8129.
[6] A.J.J. Bos, Rad. Meas. 41 (2007) S45.
[7] A.J.J. Bos, Materials 10 (2017) 1357.
[8] S.W.S. McKeever, Thermoluminescence of Solids, Cambridge University Press, Cambridge, 1985.
[9] P. Dorenbos, J. Phys.: Condens. Matter 15 (2003) 8417.
[10] P. Dorenbos, Phys. Rev. B 85 (2012) 165107.
[11] M. Back, E. Trave, N. Mazzucco, P. Riello, A. Benedett, Nanoscale 9 (2017) 6353.
[12] Lin Liu, Shanshan Peng, Yuxuan Guo, Ye Lin, Xia Sun, Liang Song, Junpeng Shi, Yun Zhang, ACS Appl. Mater. Interfaces 14 (2022) 41215.
[13] Malgorzata Sojka, Carlos D.S. Brites, Luis D. Carlos, Eugeniusz Zych, J. Mater. Chem. C 8 (2020) 10086.
[14] C.K. Jørgensen, Mol. Phys. 5 (1962) 271.
[15] C.K. Jørgensen, Modern Aspects of Ligand Field Theory, North-Holland Publishing Company, Amsterdam, 1971.
[16] P. Dorenbos, J. Lumin. 214 (2019) 116536.
[17] P. Dorenbos, J. Lumin. 222 (2020) 117164.
[18] P. Dorenbos, J. Lumin. 135 (2013) 93.
[19] P. Dorenbos, J. Lumin. 136 (2013) 122.
[20] P. Dorenbos, Phys. Rev. B 87 (2013) 035118.
[21] R.D. Shannon, Acta Crystallogr. Sect. A: Cryst. Phys. Diffr. Theor. Gen. Crystallogr. 32 (1976) 751.
[22] P. Dorenbos, Opt. Mater. 69 (2017) 8.
[23] P. Dorenbos, J. Lumin. 269 (2024) 120443.
[24] A.J.J. Bos, P. Dorenbos, A. Bessiere, B. Viana, Rad. Meas. 43 (2008) 222.
[25] A.J.J. Bos, N.R.J. Poolton, J. Wallinga, A. Bessiere, P. Dorenbos, Rad. Meas. 45 (2010) 343.
[26] A.J.J. Bos, P. Dorenbos, A.Q. Bessiere, A. Lecointre, M. Bedu, M. Bettinelli, F. Piccinelli, Rad. Meas. 46 (2011) 1410.
[27] A. Lecointre, A. Bessiere, A.J.J. Bos, P. Dorenbos B. Viana, S. Jacquart, J. Phys. Chem. C 115 (2011) 4217.
[28] Ivan I. Vrubel, Vasilii Khanin, Markus Suta, Roman G. Polozkovde, Evgeniia D. Cherotchenko, Phys. Chem. Chem. Phys. 25 (2023) 18364.
[29] Guojun Gao, Andrey Turshatov, Ian A. Howard, Dmitry Busko, Reetu Joseph, Damien Hudry, Bryce S. Richards, Adv. Sustain. Syst. 1 (2017) 1600033.
[30] Koen Van den Eeckhout, Adrie J.J. Bos, Dirk Poelman, Philippe F. Smet, Phys. Rev. B 87 (2013) 045126.
[31] J. Ueda, P. Dorenbos, A.J.J. Bos, K. Kuroishi, S. Tanabe, J. Mater. Chem. C 3 (2015) 5642.

[32] Ang Feng, Jonas J. Joos, Jiaren Du, Philippe F. Smet, Phys. Rev. B 105 (2022) 205101.
[33] Yuuki Kitagawa, Jumpei Ueda, Setsuhisa Tanabe, Phys. Stat. Sol. A (2022) 2100670.
[34] G. Kitis, J.M. Gomez-Ros, Nucl. Instrum. Methods A 440 (2000) 224.
[35] P. Dorenbos, J. Lumin. 267 (2024) 120358.
[36] A.H. Krumpel, E. van der Kolk, D. Zeelenberg, A.J.J. Bos, K.W. Kramer, P. Dorenbos, J. Appl. Phys. 104 (2008) 073505.
[37] Tianshuai Lyu, Pieter Dorenbos, J. Mat. Chem. C. 6 (2018) 369.
[38] S.M.V. Novais, Caracterizacao Estrutural E Optica Do Composto $NaYP_2O_7$ Dopado Com Terras-Raras (Thesis), Federal University of Sergipe, Brazil, 2014.
[39] A.H. Krumpel, A.J.J. Bos, A. Bessiere, E. van der Kolk, P. Dorenbos, Phys. Rev. B 80 (2009) 085103.
[40] H.F. Brito, J. Hassinen, J. Holsa, H. Jungner, T. Laamanen, M. Lastusaari, M. Malkamaki, J. Niittykoski, P. Novak, L.C.V. Rodrigues, J. Therm. Anal. Calorim. 105 (2011) 657.
[41] Y. Katayama, T. Kayumi, J. Ueda, P. Dorenbos, B. Viana, S. Tanabe, J. Mater. Chem. C 5 (2017) 8893.
[42] Tianshuai Lyu, Pieter Dorenbos, Appl. Phys. Rev. 11 (2024) 011415.
[43] T. Lyu, P. Dorenbos, Chem. Mater. 32 (2020) 1192.
[44] Wenxiang Wang, Zhenyu Sun, Xiaoyang He, Yudong Wei, Zehua Zou, Jiachi Zhang, Zhaofeng Wang, Zhiya Zhang, Yuhua Wang, J. Mater. Chem. C 5 (2017) 4310.
[45] T. Aitasalo, J. Holsa, M. Kirm, T. Laamanen, J. Niittykoski, J. Raud, R. Valtonen, Rad. Meas. 42 (2007) 644.
[46] Tianshuai Lyu, Pieter Dorenbos, Chem. Eng. J. 400 (2020) 124776.
[47] Jian Xu, Jumpei Ueda, Setsuhisa Tanabe, Opt. Mater. Express 5 (2015) 963.
[48] Jumpei Ueda, Shun Miyano, Jian Xu, Pieter Dorenbos, Setsuhisa Tanabe, Adv. Photonic Res. 2 (2021) 2000102.
[49] Jumpei Ueda, Ryomei Maki, Setsuhisa Tanabe, Inorg. Chem. 56 (2017) 10353.
[50] Zhenbin Wang, Wenxiang Wang, Jiachi Zhang, Xin Ji, Jianpeng Li, Jian Liang, Shanglong Peng, Zhipeng Ci, Yuhua Wang, Opt. Mater. Express 6 (2016) 1186.
[51] Jian Xu, Jumpei Ueda, Setsuhisa Tanabe, J. Am. Ceram. Soc. 100 (2017) 4033.
[52] Jumpei Ueda, Shun Miyano, Setsuhisa Tanabe, ACS Appl. Mater. Interfaces 10 (2018) 20652.
[53] Chuan Liao, Hao Wu, Huajun Wu, Liangliang Zhang, Guo-hui Pan, Zhendong Hao, Feng Liu, Xiao-jun Wang, Jiahua Zhang, Laser Photonics Rev. (2023) 2300016.
[54] Fangtian You, A.J.J. Bos, Qiufeng Shi, Shihua Huang, P. Dorenbos, Phys. Rev. B. 85 (2012) 115101.
[55] Yumiko Katayama, Hiroaki Kobayashi, Jumpei Ueda, Bruno Viana, Setsuhisa Tanabe, Opt. Mater. Express 6 (2016) 257134.
[56] Hongde Luo, Adrie J.J. Bos, Pieter Dorenbos, J. Phys. Chem. C 120 (2016) 5916.
[57] H. Luo, A.J.J. Bos, A. Dobrowolska, P. Dorenbos, Phys. Chem. Chem. Phys. 17 (2015) 15419.
[58] Yixi Zhuang, Ying Lv, Le Wang, Wenwei Chen, Tian-Liang Zhou, Takashi Takeda, Naoto Hirosaki, Rong-Jun Xie, ACS Appl. Mater. Interfaces 10 (2018) 1854.
[59] Tianshuai Lyu, Pieter Dorenbos, Zhanhua Wei, Chem. Eng. Journal 461 (2023) 141685.
[60] L.C. Oliveira, E.G. Yukihara, O. Baffa, Sci. Rep. 6 (2016) 24348.
[61] L.C. Oliveira, E.G. Yukihara, O. Baffa, J. Lumin. 209 (2019) 21.
[62] Yixi Zhuang, Ying Lv, Ye Li, Tianliang Zhou, Jian Xu, Jumpei Ueda, Setsuhisa Tanabe, Rong-Jun Xie, Inorg. Chem. 55 (2016) 11890.
[63] Y. Miyamoto, H. Kato, Y. Honna, H. Yamamoto, K. Ohmi, J. Electrochem. Soc. 156 (2009) J235.
[64] K. van den Eeckhout, P.F. Smet, D. Poelman, J. Lumin. 129 (2009) 1140.
[65] Tianshuai Lyu, Pieter Dorenbos, Chem. Eng. J. 372 (2019) 978.
[66] E.D. Milliken, L.C. Oliveira, G. Denis, E.G. Yukihara, J. Lumin. 132 (2012) 2495.
[67] Atsunori Hashimoto, Jumpei Ueda, Yasushi Aoki, Pieter Dorenbos, Setsuhisa Tanabe, J. Phys. Chem. C 127 (2023) 15611.